

# Mechanical properties and immunotherapeutic effects of dissolving microneedles with different drug loadings based on hyaluronic acid

Dazhi Wang<sup>1#</sup>, Meihua Jiang<sup>1#</sup>, Xiaowen Wang<sup>1</sup>,  
Chen Wang<sup>1</sup>, Xiaoyu Ou<sup>1</sup>, Lei Shang<sup>1,2\*</sup>

<sup>1</sup>School of Pharmacy, Shenyang Medical College, Shenyang, People's Republic of China,

<sup>2</sup>Suzhou biomedical Research & Development Center, Suzhou, People's Republic of China

<sup>#</sup>These authors contributed equally to this manuscript.

Improving vaccine immunity and reducing antigen usage are major challenges in the clinical application of vaccines. Microneedles have been proven to be painless, minimally invasive, highly efficient, and have good patient compliance. Compared with traditional transdermal drug delivery, it can effectively deliver a large-molecular-weight drug into the skin, resulting in a corresponding immune response. However, few studies have examined the relationship between microneedle loading dose and immune effects. In this study, the hyaluronic acid (HA) conical and pyramidal dissolving microneedles were prepared by the two-step vacuum drying method, respectively. The model drug ovalbumin (OVA) was added to HA to prepare dissolving microneedles with different loading amounts. The mass ratios of HA to OVA were 5:1, 5:3, and 5:5. The mechanical properties of the dissolving microneedles were characterized using nanoindentation and *in vitro* puncture studies. The immune effects of the matrix and drug content were studied in Sprague–Dawley (SD) rats. Finally, the diffusion behavior of OVA and the binding mode of HA and OVA in the microneedles were simulated using Materials Studio and Autodocking software. The experimental results showed that the conical microneedles exhibited better mechanical properties. When the mass ratio of HA to OVA was 5:3, the immune effect can be improved by 37.01% compared to subcutaneous injection, and achieved a better immune effect with relatively fewer drugs. This conclusion is consistent with molecular simulations. This study provides theoretical and experimental support for the drug loading and efficacy of microneedles with different drug loadings.

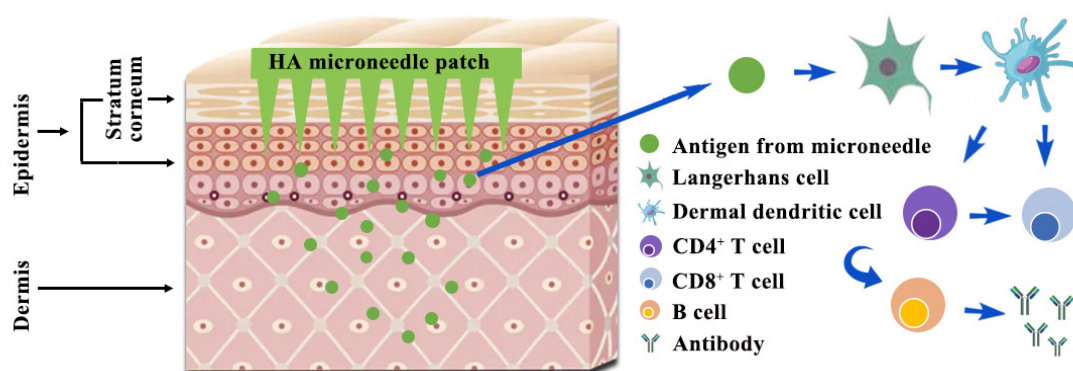


**FIGURE 1** - Schematic presentation of HA microneedle action.

**Keywords:** Immunization. Hyaluronic acid microneedle. Molecular dynamics simulation. Diffusion coefficient.

\*Correspondence: Lei Shang, Shenyang Medical College, 146 Huanghe North Street Shenyang 110034, Liaoning, People's Republic of China. Phone: +86 13080858366. E-mail: shanglei6677@163.com. ORCID: <https://orcid.org/0000-0003-2805-787X>

## INTRODUCTION

Immunotherapy has been widely investigated as a promising cancer treatment strategy (Kim *et al.*, 2019). In immunotherapy, the skin is an attractive target for vaccination because it is an active immune-competent organ (Wamhoff *et al.*, 2019). More importantly, the skin is the largest organ of the human body (Wang *et al.*, 2020), with several types of antigen-presenting cells (APCs) and immunologically active accessory cells (Kim *et al.*, 2018; Leone *et al.*, 2019) such as Langerhans cells (LCs) and dermal dendritic cells (DCs) (Kim *et al.*, 2018). They capture antigens and migrate to draining lymph nodes for antigen presentation to T cells, evoking antigen-specific T-cell and B cell activation (Leone *et al.*, 2019).

Transcutaneous delivery is ideal for transporting therapeutic reagents or vaccines to the skin (Chiu *et al.*, 2021). Compared to traditional intramuscular and subcutaneous injections, percutaneous immunization has many advantages. Percutaneous immunization can increase the contact probability and duration between antigens and immune cells, resulting in a more effective and long-lasting immunization (Balmert *et al.*, 2020; Li *et al.*, 2017). However, the stratum corneum (SC) poses a barrier to the entry of many therapeutic entities (Li *et al.*, 2021), and few drugs with specific physicochemical properties can be effectively administered via the transdermal route (Dharadhar *et al.*, 2019). Proteins usually exhibit relatively low transdermal delivery efficacy because of their high molecular weight, distinct hydrophilicity, and charged states (Zhu *et al.*, 2020). To increase the permeability of proteins, various enhancement technologies, such as iontophoresis, sonophoresis, electroporation, thermal ablation, and newer synergistic techniques, have been developed in recent decades. However, these approaches are invasive, have low bioavailability, or require special apparatus, which is unacceptable in clinical settings (Vora *et al.*, 2020).

Microneedles (MNs) are a novel transdermal drug delivery technology that is more effective and safer than traditional transdermal drug delivery systems (Zhan *et al.*, 2018). MNs have been applied in many fields, such as the controlled release of insulin, vaccines, and

treatment of eye diseases and so on (Hao Feng *et al.*, 2020; Zhuang *et al.*, 2020). Microneedles are needle-like structures with dimensions less than 1 mm (van der Maaden *et al.*, 2018). Because of their miniature dimensions, MNs can pierce through the SC but fail to reach nerve endings and thus do not elicit pain (Dharadhar *et al.*, 2019). They can effectively deliver active drugs to the dermis layer in a minimally invasive and painless manner, improving patient acceptability and compliance, and reducing the risk of cross-infection (Du *et al.*, 2019; van der Maaden *et al.*, 2018; Zhu *et al.*, 2020). There are many different types of MNs, such as hollow MNs, solid, dissolving, and swelling MNs (Anderson *et al.*, 2019; Zhan *et al.*, 2018). Among the various types of MNs, dissolving MNs (dMNs) have attracted increasing attention because of their easy preparation and improved safety (Li *et al.*, 2017). The advantages of dMNs include the absence of sharp needle waste and the risk of leaving harmful materials on the skin (Leone *et al.*, 2019). In addition, dMNs perform well in precisely controlling drug release and delivery ((Ahmed Saeed Al-Japairai *et al.*, 2020). The ideal material for dMNs should be safe, compatible with the payload, easy to handle during preparation, and have sufficient mechanical strength for skin penetration (Monkare *et al.*, 2015).

Hyaluronic acid (HA) is a polyanionic disaccharide comprising N-acetyl-D-glucosamine and D-glucuronic acid. Each repetitive disaccharide unit is linked by  $\beta$ -1,4-glycosidic bonds (Saha, Rai, 2021). It is ubiquitously present in the body and the skin HA accounts for 50% or more of the total (Zhu *et al.*, 2020). As an FDA-approved biocompatible material, HA possesses unique viscoelasticity, biocompatibility, biodegradability, and nonimmunogenicity. HA has been successfully used in knee adhesive replacement, ophthalmic surgery, and drug delivery (Saha, Rai, 2021). Compared to other polymers, HA microneedles (HA-MNs) have several advantages, such as receptor-based drug delivery processes, skin hydration, hydrophobic interactions with SC, bioadhesion, and viscoelastic (Zhu *et al.*, 2020). HA-MNs can penetrate the epidermis without disrupting the skin cell viability or inducing an inflammatory response (Zvezdin *et al.*, 2020).

Generally, the drug release pattern depends on many factors, including the drug-binding affinity, molecular weight, and rate of hydration of the polymer material. High-molecular-weight HA (HMw-HA, Mw=1800–2200 kDa) is relatively viscous in aqueous solutions and takes a long time to metabolize in the human body, with better viscoelasticity, cohesion, and film-forming properties. Medium-molecular-weight HA (MMw-HA, Mw=1000 k~1800 kDa) exhibits strong lubricating and moisturizing properties. Low molecular weight HA (LMw-HA, Mw=10–1000 kDa) has strong skin penetration and is quickly metabolized in the human body (Essendoubi *et al.*, 2016; Hoarau, Polette, Coraux 2022; La Gatta *et al.*, 2020). Therefore, low-molecular-weight HA is a suitable matrix material for dMNs.

In addition, researchers have investigated the effects of different molecular weights and HA concentrations on the structure of MNs. Their study showed that the molecular weight of HA had no effect on the puncture performance of MNs and that a high molecular weight of 150 kDa HA decreased MNs solubility (Leone *et al.*, 2020). A microneedle prepared with 10% HA as the matrix did not create a cavity at the tip, and if the concentration is too large the solution would be viscous and difficult to handle (Leone, *et al.*, 2019). MNs can generate stronger immune responses at smaller doses than conventional subcutaneous injections. Kim *et al.* (2019) developed a low molecular weight HA-MNs (Mw=17 kDa) that successfully delivered antigen peptides to the body and significantly inhibited the melanoma tumor growth. However, the diffusion behavior of macromolecular drugs in MNs and the effect of different drug loadings on immune responses have not been well studied.

In this study, HA (Mw=10 k) and ovalbumin (OVA) were selected as the matrix and model drugs, respectively, to prepare dMNs using a two-step vacuum drying method. The mechanical properties of dMNs with different shapes were studied in detail using nanoindentation and mathematical analyses. In addition, we focused on the immune responses induced by different ratios of drug-loaded microneedles and the relationship between the drugs and polymers. Ultimately, the *enzyme-linked* immunosorbent assay (ELISA) results

and molecular dynamics simulations determined that HA: OVA=5:3 (w/w) in dMNs resulted in a better concentration of the model drug at the needle tip and produced stronger immune effects than conventional intravenous injections. Thus, this study provides a new approach for immunodelivery of macromolecular drugs.

## MATERIAL AND METHODS

### Material

HA (CAS:9004-61-9, average molecular weight =10 kDa) was purchased from Shanghai Ryon Biological Technology, Ltd. (Shanghai, China). OVA (CAS:9006-59-1) was obtained from Shanghai Acme Biochemical Co. Ltd. (Shanghai, China). Methylene blue trihydrate (CAS:7220-79-3,  $C_{16}H_{18}ClN_3S \cdot 3H_2O \geq 98.5$ ) was purchased from Xilong Scientific Co., Ltd. (Guangzhou, China). The (PDMS) micromolds were obtained from Huadu District Laike Mold Firm (Guangzhou, China) and contained two shapes (pyramidal and conical). Other instruments consisted of a biomicroscope (Otter Optics B302, Chongqing Ott Optical Instruments Co., Ltd., Chongqing, China), a DF-101S collector-type constant-temperature heating magnetic stirrer (Gongyi Yuhua Instrument Co., Ltd, Gongyi, China), and a sand vacuum drying oven (DZF-6051, Shanghai Yiheng Scientific Instruments Co., Ltd., Shanghai, China). All other reagents used were of reagent grade, and all solvents were of analytical grade.

### Animals

Sprague–Dawley (SD) rats (6 weeks old, 200 ± 20 g) were purchased from Liaoning Changsheng Biotechnology Co., Ltd. All animals were maintained under standard temperature/lighting conditions and provided with food and water ad libitum. Porcine ear skin samples were obtained from a local slaughterhouse. The hair on the ears and subcutaneous adipose tissue were shaved. Ear skin samples were collected and stored at –80°C until being processed. This study was approved by the Ethics Committee of Shenyang Medical College (Shenyang, China).

## Dissolving microneedles

### Hyaluronic acid microneedle fabrication

To improve the utilization of drugs carried by dMNs and reduce waste, a two-step casting method was used to prepare dMNs. For the dMNs preparation, HA solution (10% w/v) was prepared in distilled water with stirring at 1800 rpm at room temperature for 30 min. The solution was left for 10 min to remove air bubbles. The DMNs patches were fabricated using a gating

process. Poured 10% HA solution onto pyramidal and conical PDMS molds, separately. To make sure free of bubble at the tip of the needle, the solution was transferred into a vacuum drying oven and dried for 10 min at -100 kPa. The HA solution was then added again to each mold. Subsequently, the mold was placed in a vacuum drying oven (-42 kPa, 313 K □ for 24h until the solution of the microneedle solution completely dried. After desiccation, the patch was carefully separated from the PDMS mold. The workflow is illustrated in Figure 2.

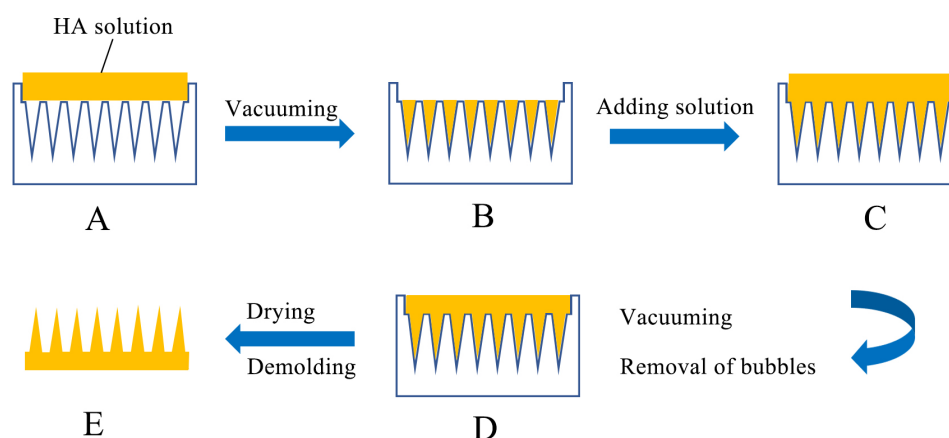


**FIGURE 2** - Preparation of dissolving microneedles using two-step vacuum drying method.

### HA-OVA microneedle fabrication

OVA was added to 10% HA solution and the addition ratio is HA:OVA = 5:1 □ 5:3 □ 5:5 □ w/w □. The mixture was stirred at 1800 rpm for 30 min. The procedure for Hyaluronic acid microneedle fabrication was repeated. The HA-OVA microneedles patches were carefully removed after drying.

### Methylene blue trihydrate microneedle preparation

Methylene blue trihydrate was added to the mixture of HA and OVA. The procedure for Hyaluronic acid microneedle fabrication was repeated. Finally, the arrays were removed from the PDMS mold and stored in a desiccator at room temperature in a desiccator until use.

## Characterization of dissolving microneedle patches

### Microneedle patch appearance

The biomicroscope was chosen to observe the characterization of HA microneedles.

### Microneedle mechanical strength assessment

The needle length of the pyramidal and conical molds in this research are both 600 μm, the bottom side length of the pyramidal microneedle is 290 μm, and the bottom diameter of the conical microneedle is 230 μm. To deliver drugs to the skin, MNs must possess suitable mechanical properties. The normal stresses of the two MNs during the pressurization process were

calculated according to the Figure 3 model. The normal stress was calculated by dividing the compressive force by the top contact area. where  $r_1$  is the bottom radius of the conical microneedle,  $r_2$  is the top radius of the conical microneedle during forced deformation,  $r_3$  is half the diagonal of the bottom of the pyramidal microneedle,  $r_4$  is half the diagonal of the top of the pyramidal microneedle during forced deformation, and  $H$  is the initial height of the pyramidal and conical microneedles.  $\delta$  is the longitudinal displacement distance of the microneedle during the stress process. According to the principle of geometric similarity, we can obtain Eq. (1) and Eq. (2), and then obtain the relationship between the top area of cone ( $s_1$ ) and pyramid ( $s_2$ ) and the change in displacement ( $\delta$ ), namely Eq. (3) and Eq. (4).

$$\frac{H}{\delta} = \frac{r_1}{r_2} \quad (1)$$

$$\frac{H}{\delta} = \frac{r_3}{r_4} \quad (2)$$

$$S = \frac{\pi \cdot (r_1 \cdot \delta)^2}{H^2} \quad (3)$$

$$S = \frac{2 \cdot (r_3 \cdot \delta)^2}{H^2} \quad (4)$$

The normal stress is equal to the pressure applied to the top of the tip divided by the area of the top of the microneedle after deformation by force.

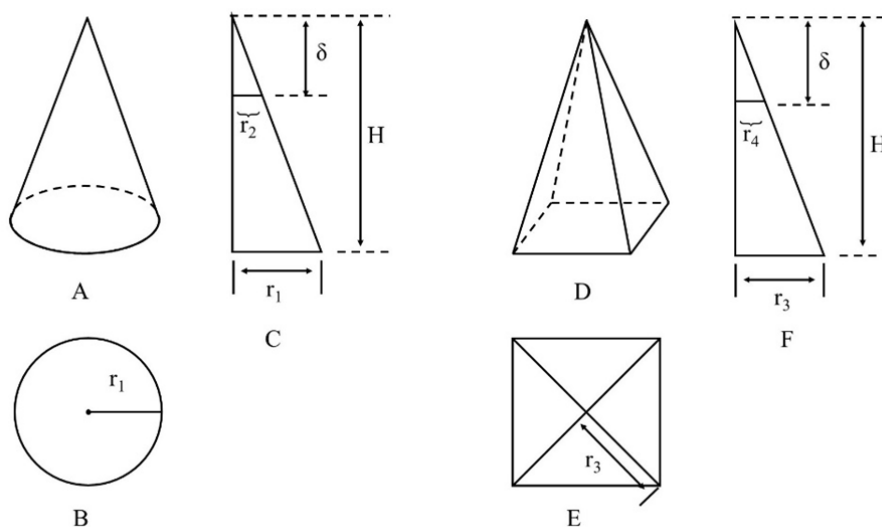


**FIGURE 3** - Schematic diagram of the pyramidal and conical microneedle mathematical model. **A** Conical microneedle model. **B** Top view of conical microneedle model. **C** Longitudinal section of conical microneedle model. **D** Pyramidal microneedle model. **E** Top view of pyramidal microneedle model. **F** Longitudinal section of pyramidal microneedle model.

In order to verify the calculation results and better evaluate the mechanical properties of MNs, nanoindentation instrument (CSM, Switzerland, TI-950) was used to perform mechanical properties of the MNs. Two types of 10% HA-MNs were tested in nanoindentation experiments. Pressure

was gradually applied at 50 mN at a constant speed of 120.0 mN/min in the vertical direction of the needle tip, and a force of 50 mN was continuously applied for 10 s. Finally, the deformation of the microneedle was calculated using the following formula:

Degree of deformation (%) =

$$= \frac{\text{Compression deformation length}}{600\mu\text{m}} * 100 \quad (5)$$

#### Microneedle puncture capability assessment

Porcine skin is often used as a model of human skin because of its similarities in anatomy and physiology (Zhan *et al.*, 2018). Porcine ear skin (700  $\mu\text{m}$ ) was used for the *ex vivo* puncture experiments. The subdermal tissue was removed using scissors and kept at  $-20^\circ\text{C}$  for reserve. With the SC of the porcine ear facing upwards, the dMNs were pressed for at least 1 min and then removed. The puncture site was imaged using a biological microscope (Ott Optics, B302) and the number of methylene blue-stained pinholes at the puncture site was calculated. The MNs puncture efficiency was calculated according to Eq. (6).

$$\text{Penetration efficiency (\%)} = \frac{\text{Number of blue spots}}{400} * 100 \quad (6)$$

#### *In vivo* microneedle dissolution experiment

To determine the dissolution time of dMNs *in vivo*, the rats were anesthetized with an intraperitoneal injection of 20% urea. The hair on the back was then shaved. The dMNs were pressed continuously with the thumbs to ensure that they did not detach from the backs of the rats during the experiment. The dMNs patches were removed after 1, 2, 4, 6, 8, and 10 min to observe the dissolution of the dMNs.

#### Simulation of OVA distribution and diffusion in HA microneedles

In this study, dissipative particle dynamics (DPD) simulations were performed to study the diffusion rate of OVA in different proportions of HA solution. Mean square displacement (MSD) analysis was performed to calculate the translational diffusion coefficient, which was used to study the diffusion of OVA in different ratios of HA solutions. In an infinitely short time, the slope of a point on the MSD curve is proportional to the change in

the point relative to the initial position. A larger MSD value indicates a greater range of motion of OVA in solution and greater diffusivity.

Diffusion coefficient:

$$D = \frac{1}{6N_a} \lim_{t \rightarrow \infty} \frac{d}{dt} \sum_{i=1}^{N_a} [r_i(t) - r_i(0)]^2 \quad (7)$$

The radial distribution function (RDF) represents how the density of a particle varies as a function of its distance from a reference particle and can be used to simulate the HA distribution around the OVA. In a particle system, the RDF is a measure of probability and is typically expressed as  $g(r)$ . RDF was explained as the probability of locating particle "O" within the range  $(r+dr)$  of particle A. In this study, OVA was used as the localization atom. The larger  $\rho_g(r)$  indicates the more HA around OVA, namely, the more uniformly the OVA is distributed in the HA. When OVA was more evenly distributed and diffused faster in HA MN, it produced a better immune effect. All computational calculations were performed using Materials Studio software package.

Radial distribution function:

$$g_{AB}(r) = \frac{1}{\rho_{AB} 4\pi r^2} \frac{\sum_{i=1}^K \sum_{j=1}^{N_{AB}} \Delta N_{AB}(r \rightarrow r + \delta r)}{N_{AB} \times K} \quad (8)$$

#### Microneedle Immunization Experiment

The rats were randomly divided into three groups: control, subcutaneous injection, and MNs groups. There were four animals in each group. The MNs group was divided into HA-MNs, HA:OVA=5:1-MNs, HA:OVA=5:3-MNs, and HA:OVA=5:5-MNs, respectively; Subcutaneous injection group was injected intraperitoneally with OVA (12  $\mu\text{g}/\text{mL}$ , 1 mL). The control group was injected intraperitoneally with saline (0.9% NaCl; 1 mL). The groupings are listed in Table I. The back skin of the rats was shaved one day before the experiment. The rats were fasted for 24 hours and

provided with access to clean water. In the MNs group, different dMNs were applied to the back skin of rats for 8 min to ensure complete dissolution of dMNs. Primary and booster immunizations were performed at weeks 1 and 3, respectively. Rats were monitored at week 1,2,3,4 and collected one milliliter of blood was collected. After precipitated, the blood sample was centrifuged for 15 minutes (3000 r/min, 4°C) by a high-speed centrifuge (Thermo BIOFUGE STRATOS).

**TABLE I** - Animal Experiment Group

Drug delivery methods	Immunization method
MNs	HA:OVA=5:1-MNs
	HA:OVA=5:3-MNs
	HA:OVA=5:5-MNs
	Control HA-MNs
Subcutaneous injection	OVA
Control	Saline

### Serum IgG protein analysis

The titer of OVA-specific immunoglobulin G (IgG) antibody was assessed using ELISA. The antibody-coated 96-well plates were removed, and standard, sample, and blank control wells were set. The standard and sample to be tested were added to pre-coated 96-well plates with rat IgG capture antibodies. Add 50 µL of standards (0.5, 1, 2, 4, 8, 16 mg/mL) to the standard wells and 50 µL serum added to the sample wells. 100 µL of horseradish peroxidase labeled IgG antibody was added to each well and the sample was incubated in a 37°C warm bath for 60

min. Thereafter, each well was thoroughly dried with absorbent paper after washing five times with a diluted washing solution. After washing, 100 µL of 3, 30, 5, 50-tetramethylbenzidine (TMB) substrate was added and light avoidance incubation for 15 min for color development. A stop solution was added to terminate the reaction. Absorbance was measured at 450 nm using a BioTek Biomarker (BioTek, USA) within 15 min. Serum antibody concentrations were calculated from the standard curves and expressed as µg/mL.

### Statistics Analysis

All data were analyzed using Origin 2018, and *P* values less than 0.05 were considered statistically significant.

## RESULTS AND DISCUSSION

### Microneedle morphology characterization

The two-step preparation of dMNs allows for better concentration of the drug at the tip of the needle and achieves a concentrated distribution of the drug at the tip (Zhuang *et al.*, 2020). In this paper, we successfully fabricated pyramidal and conical type of dMNs with the height of 600 µm by a two-step vacuum drying method. Figure 4A shows the structure and dimensions of conical and pyramidal single microneedles and microneedle arrays observed using a biomicroscope. As shown in the Figure 4A, both dMNs are 20\*20 arrays with a height of 600 µm, and a base diameter of the conical dMNs is 230 µm, and a base diameter of the pyramidal dMNs is 290\*290 µm. Each dMNs array comprised 400 single microneedles. According to Figure 4A, all dMNs had smooth surfaces and complete needle tips.

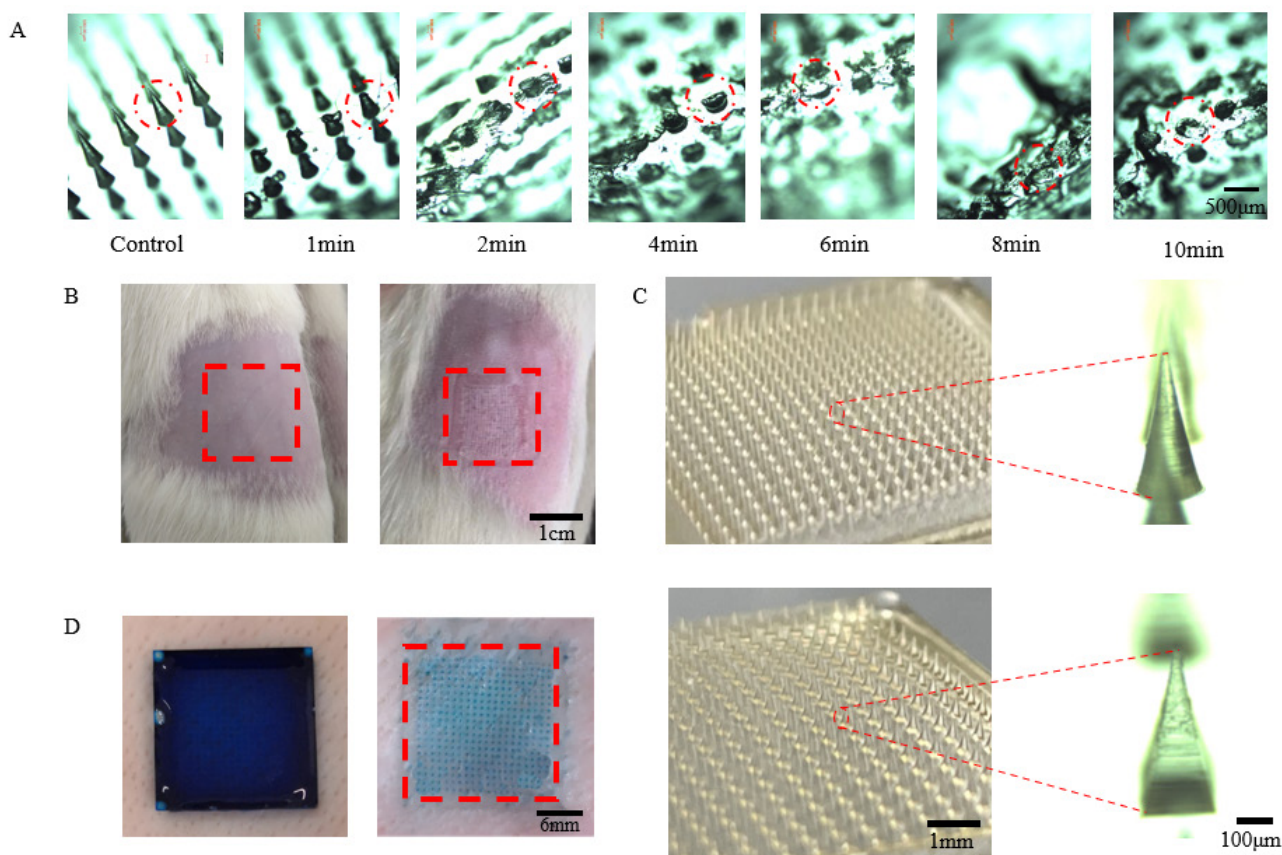


**FIGURE 4** - Characterization of dMNs. **A** Representative light microscope images of dMNs before dissolution (0 min) and after 1, 2, 4, 6, 8 and 10 min dissolution in SD rat skin (40x). **B** Visual examination of dorsal skin appearance before and after microneedle treatment. **C** Structure and dimensions of conical and pyramidal single microneedle and microneedle arrays. **D** Penetration of methylene blue stained microneedles into porcine ear skin.

During the preparation process, the effects of air bubbles, vacuum pressure, drying temperature and time affect the dMNs drying procedure. In our experiments, certain phenomena will occur if there are bubbles in the solution and the vacuum pressure is lower than the optimum pressure, some things will happen. 1. During the drying process, there may be bubbles in the dMNs backing layer, which will make it broken and unable to form. 2. The backing layer changed from horizontal to convex, making it impossible to prepare dMNs with a good morphology. This is because, during the drying process, the bubbles present in the raw solution concentrate in the backing layer and sharply reduce the mechanical properties of the dMNs (Zhuang *et al.*, 2020). When the temperature increased above the optimum temperature,

the drying time of the dMNs was significantly shortened, and the forming quality was greatly affected, including: 1. When the temperature was excessively high, the dMNs were fragile and could not be completely removed from the mold. 2. A large number of air bubbles appear in the backing layer of the dMNs, drastically reducing their mechanical properties. When the drying temperature was too low, the backing layer bent and required longer drying times. Theoretically, a higher drying temperature leads to more intense molecular motion in the solution, resulting in shorter fabrication periods. However, too high a temperature would affect the stability of the drugs, and the fabricated dMNs would present serious warpage after demolding owing to the residual stress concentration. Although drying at low temperatures can

preserve antigen stability, it may lead to a long processing time that is incompatible with scalability in fabrication and to a higher residual moisture content in dMNs than drying at high temperatures, potentially resulting in a decrease in antigen stability (Leone *et al.*, 2019; Leone *et al.*, 2020; Zhuang *et al.*, 2020).

### **In vivo dissolution and performance characterization**

Good mechanical properties are critical for MNs to overcome the skin barrier and achieve efficient transdermal drug delivery. This is because it determines the efficiency and reliability of drug penetration after the topical application of MNs. As shown in Figure 3, a mathematical model was used to characterize the forces acting on the pyramids and cones. In this model, we assumed that the deformation of the MNs backing layer was negligible, because the height of the microneedle tip was much larger than that of the backing layer. When pressure was applied to the tips of the pyramids and cones to simulate skin puncture, the height of the MNs was reduced owing to the force, and the top area increased. According to Eq. (3) and Eq. (4), when the displacement is the same, the top area of the conical MNs is smaller than that of the pyramidal MNs, which can generate a larger normal stress. Therefore, the same external pressure was applied, and the displacement distance of the conical MNs was smaller. As MNs require the same amount of pressure to penetrate the skin, the simulation results showed that conical MNs can produce less deformation than pyramidal MNs. This conclusion was also confirmed in nanoindentation experiments. The mechanical properties of the different forms of dMNs were observed by nanoindentation, and the results are shown in Figure 5. A displacement curves of needles of two different shapes were plotted. The curves of OA and OY were obtained by gradually applying 50.0 mN pressure at a constant speed of 120.0 mN/min in the vertical direction of the needle tip with the nanoindentation head. The curves YB<sub>1</sub> and AB<sub>2</sub> were the holding sections, where a force of 50.0 mN was applied for 10 s. During the loading process, the same load of 50.0 mN was gradually applied to the tips of the two types of dMNs. The OY and OA curves

represent the relationship between the loads on the tips of the conical and pyramidal dMNs and the compression deformation of the tips. The slope represents the elastic modulus of the corresponding dMNs. As shown in Figure 5, the slope relationship of the two curves is OY>OA, indicating that the elastic modulus relationship of the two types of dMNs is cone>pyramid. It can be seen from the load-displacement curves of the nanoindentation that with an increase in pressure, there is no excessive point in the curve. This indicates that the dMNs have good compression resistance.

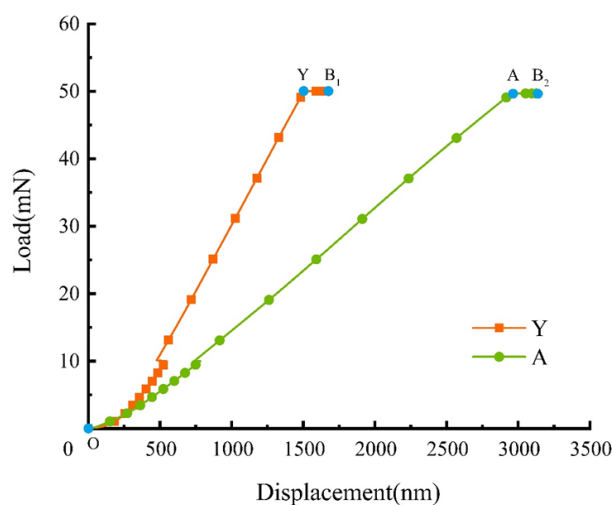


**FIGURE 5** - The load-displacement curves of pyramidal and conical microneedle HA microneedles tested using nanoindentation. Curve OA,OY indicates the loading section, Curve AB<sub>2</sub>, YB<sub>1</sub> indicates the holding section. A: Pyramidal Microneedle. Y: Conical Microneedle.

The minimum pressure for the dMNs puncture skin puncture was 10.0 mN (Zhuang *et al.*, 2020). When the pressure of 10.0 mN is applied, the deformation rates of conical and pyramidal dMNs are only 0.09% and 0.13%. The nanoindentation data showed that both the conical and pyramidal structures ensured that the dMNs could penetrate the skin without fracturing. According to Eq. 5, when the same pressure of 50.0 mN was applied, the deformation rate of the conical is 0.25%, and the pyramidal is 0.50%. That is, the cone had better mechanical properties than the pyramidal cone, which is consistent with the results of the mathematical simulation analysis. In subsequent experiments, conical dMNs were selected.

To evaluate the skin penetration performance of the dMNs, the prepared MB-stained dMNs were applied to pig ears. The puncture results are shown in Figure 4B. After the dMNs application, distinct blue pinholes were observed on the porcine ear skin, indicating that the dMNs had sufficient mechanical strength. The penetration efficiency of dMNs is close to 100%. Similar results were obtained from the *in vivo* experiments. Visual examination of the dorsal skin appearance before and after dMNs treatment is shown in Figure 4C. That is, dMNs can penetrate the stratum corneum (10-20  $\mu\text{m}$ ) and release the drug into the epidermis that is rich in DCs and LCs. In our study, the skin recovered 10 min after the removal of the dMNs, indicating that there were no side effects such as skin inflammation or redness.

The dissolution time of dMNs *in vivo* is shown in Figure 4D. When dMNs were applied for 8 min, the needles were completely dissolved, and the backing layer did not change. Residual needles were still present when the application time was less than 8 min. When the time exceeded 8 min, the dMNs backing layer began to dissolve, and the structure was destroyed. Therefore, it is proven that the dMNs prepared by the above method can satisfy the application requirements well.

### Simulation of drug distribution and release in microneedles

#### *Interaction between HA and OVA*

In the HA molecule,  $\beta$ -(1 $\rightarrow$ 3)-glycosidic linkage associates D- glucuronic acid with amino-sugar and  $\beta$ -(1 $\rightarrow$ 4)-glycosidic linkage connects amino-sugar with D-glucuronic acid (Zhu *et al.*, 2020). HA is capable of interacting with various chemicals owing to the presence of both polar and non-polar groups in the HA polymer chains (Saha, Rai, 2021). They include proteins, vitamins, DNA, hydrophilic drugs, and macromolecules. HA forms hydrogen bonds with macromolecules, thereby stabilizing their solutions. HA mainly interacts with macromolecular proteins through hydrogen bonds (Feng *et al.*, 2021).

In this study, the initial protein structures were downloaded from the protein data Bank (PDB ID:1OVA). All crystallographic water molecules and other nonprotein

molecules were removed to determine the binding mode of HA to OVA. Autodocking was used to identify the binding site of HA on OVA. Prior to molecular docking, Autodocking Tools were used to add hydrogens, calculate charges, and merge the non-polar hydrogens of the protein structure. Then set docking range. In this case, molecular Docking Autodocking 4.2 was used to process the molecular docking simulations using the Lamarckian Genetic Algorithm (LGA). The docking results showed that the 69<sup>th</sup> amino acid of OVA was connected to HA via hydrogen bonding.

#### *Simulation of OVA distribution and release in microneedles*

Molecular dynamics is a computer simulation technique based on atomic and molecular interactions. Molecular simulations based on classical and equilibrium statistical mechanics have become an indispensable branch of chemical research (Feng *et al.*, 2021). The most prominent function of molecular dynamics simulation is to calculate the motion characteristics of the molecules and atoms in the system (Zhao *et al.*, 2014). Molecular simulations of the diffusion coefficient have received considerable attention (Moradi *et al.*, 2020).

In this study, molecular dynamics simulations with different modules were performed using Materials Studio 7.0 software. These include the diffusion coefficient (D) and radial distribution function (RDF) of OVA in HA-OVA solutions with different mass ratios. The HA structure was drawn using the ChemDraw software. A geometry-optimization function was used to optimize the geometry of HA, OVA, and H<sub>2</sub>O under the force field of COMPASS. The construction process of the HA-OVA solution system is illustrated in Figure 6A. The optimized structures were used to build three solution systems using an Amorphous Cell module: HA:OVA=5:1 (w/w), HA:OVA=5:3 (w/w), and HA:OVA=5:5 (w/w). The preprocessed structures were optimized and minimized to generate geometrically stable structures. A 50000-step structural optimization was carried out for the constructed structure to make it structurally relaxed. After a preliminary geometry optimization phase, the system was relaxed at 298.0 K the NVT and NVE methods at 50 ps intervals, with a time step of 1 fs. The

application of the NVE ensures that dynamic properties, such as scattering coefficients, are not biased by the system-wide algorithms used to generate a constant temperature set. After equilibration, the analyses were performed separately for MSD and RDF.

Mean square displacement (MSD) analysis was performed to calculate the diffusion coefficient. The MSD can reflect the movement of molecules. In this study, larger MSD values indicated better OVA diffusion properties. Based on the fluctuation dissipation theory of nonequilibrium statistical thermodynamics, the diffusion coefficient can be calculated according to the MSD. The diffusion coefficient is expressed in Eq.4, and the results are shown in Figure 6C. In the experimental solution, the diffusion coefficient was 0.00808 Angstrom<sup>2</sup> for the HA: OVA = 5:3 (w/w) solution and 0.00768 Angstrom<sup>2</sup>

for the HA: OVA = 5:5 (w/w) solution. The diffusivity coefficients for both solvents were similar. HA: OVA = 5:1 (w/w) solution has a diffusion coefficient of 0.02127 Angstrom<sup>2</sup>. The greater the diffusion coefficient, the stronger the movement effect of OVA and the easier it is to diffuse to the backing layer. All these results demonstrate that compared with the HA: OVA = 5:1 (w/w) solution, OVA was more likely to be concentrated at the tip of the needle in the HA:OVA=5:3 (w/w) and HA:OVA=5:5 (w/w) solutions. This was also indicated by the radial distribution functions (RDF). The RDF were calculated to elucidate the former. As shown in Figure 6D, the RDF of the HA: OVA=5:3(w/w) solution was larger than that of the HA: OVA=5:1(w/w) and HA: OVA=5:5 (w/w) solutions. The RDF results showed that HA and OVA exhibited better miscibility in the HA:OVA = 5:3 (w/w) solution.

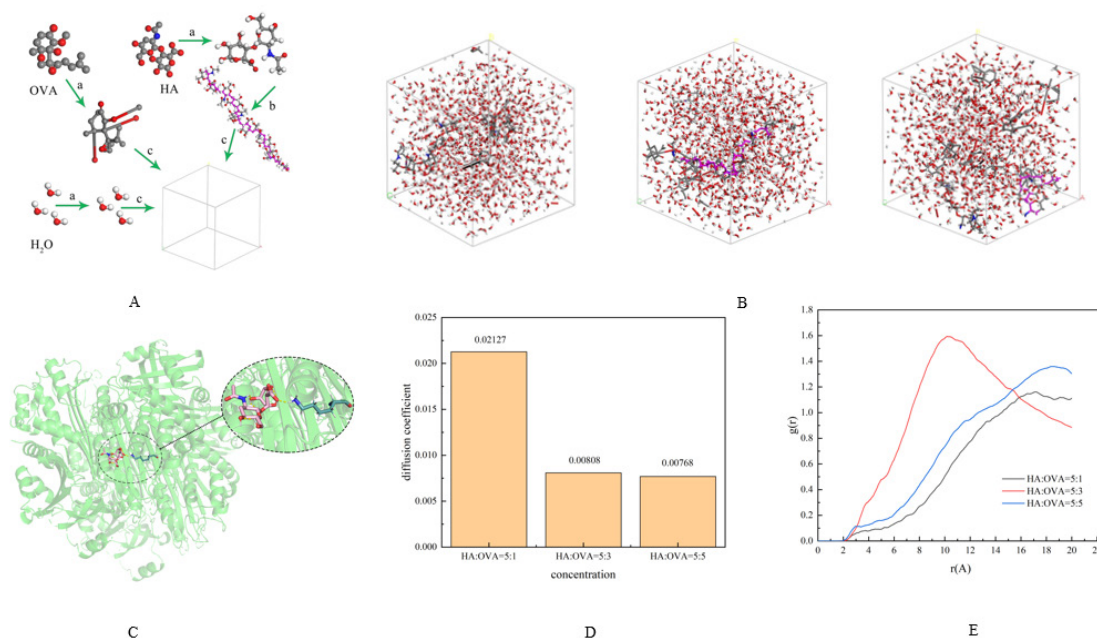


**FIGURE 6** – A: Process of HA-OVA solution construction in Material Studio. B: Conformations of minimization system of HA-OVA solution. Left, HA:OVA=5:1 (w/w) solution. Center, HA:OVA=5:3 (w/w) solution. Right, HA:OVA=5:5 (w/w) solution. C: Schematic representation of the HA docking OVA. D: MSD bar Chart of OVA in HA-OVA solution. E RDF curves of HA-OVA solution.

### ***In vivo* immune results**

The SD rats (200±20 g) were randomly divided into 6 groups (n=4) for: control group (a), subcutaneous injection group(b), and MNs group. The MNs group

was further divided into HA-dMN(c), HA:OVA=5:1-dMN(d), HA:OVA=5:3-dMN(e), and HA:OVA=5:5-dMN(f) groups. Serum from the rats was collected for the IgG enzyme immunoassay. The results are presented in Figure 7. After one week of administration, both

the OVA subcutaneous injection group and the MNs group showed enhanced concentrations of IgG-specific antibodies compared to the control group. The increase in IgG-specific antibody concentration was more pronounced in HA:OVA=5:3-dMNs and HA:OVA=5:5-dMNs group as compared to subcutaneous injection group, 4.78% and 5.04%, respectively. There was no significant difference among the subcutaneous injection, HA-dMNs, and HA:OVA=5:1-dMNs group ( $P > 0.05$ ). After two weeks of administration, subcutaneous injection group showed a considerable decrease of IgG-specific antibodies (-14.33%) and it showed significant difference compared with the MNs group ( $P < 0.05$ ). In the MNs group, the IgG-specific antibody concentrations in rats administered HA: OVA = 5:5 (w/w) dMNs showed a slight decrease (-1.07%) compared to one week after the primary immunization. However, administration of HA: OVA = 5:1 (w/w) dMNs group, HA: OVA = 5:3 (w/w) dMNs group IgG-specific antibody concentrations was still significantly enhanced (3.19%) (5.56%). After secondary immunization (three weeks), the MNs group rapidly induced an immune response. Notably, serum IgG-specific antibody concentrations dramatically increased in the MNs group compared with those in the other groups. Compared with the subcutaneous injection group, the immune effect of HA- dMNs group increased by 9.22%, HA:OVA = 5:1 (w/w) dMNs group increased by 6.73%, HA:OVA = 5:3 (w/w) dMNs group increased by 37.01%, HA:OVA = 5:5 (w/w) dMNs group increased by 39.73%. Compared to the HA-MN= 5:3 (w/w) dMNs group, the dose of OVA in the HA-OVA= 5:5 (w/w) dMNs group was increased by approximately 66.67%, but the immune effect was only increased by 2.72% after the second immunization. No significant differences were observed in the IgG-specific antibody concentrations between the HA-MN= 5:3 (w/w) dMNs and HA-OVA= 5:5 (w/w) dMNs groups ( $P > 0.05$ ). Additionally, the HA-dMNs group elicited a better immune response than the control and subcutaneous injection groups. This is because HA molecules can also activate innate immune mechanisms through CD44, CD168, Toll-like receptor (TLR)-2, and TLR-4. CD44 is a major HA receptor (Leone *et al.*, 2020). HA regulates TLR via two mechanisms. Low-molecular-weight HA

contributes to the induction of inflammation by binding to TLR2 and TLR4. Secondly, hyaluronic acid can regulate the interactions between TLR and their main ligands (Saha, Rai, 2021). Some researchers have also shown that HA can induce a strong antibody response equivalent to or better than that of a traditional injection (Chiu, Chen, Wan, 2018). These results showed that the optimal matrix-to-drug mass ratio in HA soluble microneedles was 5:3. The obtained results agree with those of molecular dynamics simulations. When the mass ratio of HA to the model drug was 5:3, the drug was more evenly distributed in the dMNs and had faster release, and a better immune effect could be achieved with relatively fewer drugs.

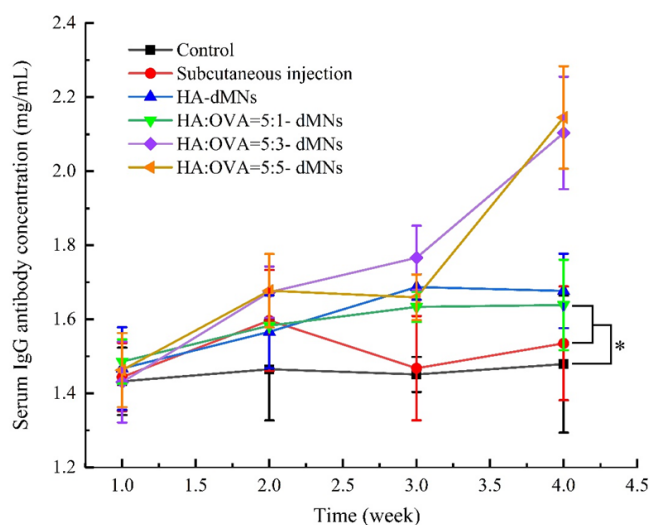


**FIGURE 7** - OVA-specific IgG1 antibody titers measured in SD mice on week 1 (prime immunization), week 2, week 3 (second immunization) and week 4. Results are shown as mean  $\pm$  SEM, compared with the control group, \* $P < 0.05$ .

In this study, low-molecular-weight HA was used as the matrix and OVA was used as the model drug to prepare microneedles using a two-step vacuum drying method. The conical dMNs have better mechanical properties than the pyramidal dMNs. Molecular simulations and immune experiments showed that, compared with other ratios, when the mass ratio of HA to the model drug was 5:3, the model drug could obtain better distribution at the tip of the needle, faster release, and a better immune effect. And its immune effect was 37.01% higher than that of subcutaneous injection. All experimental results

agree well with the simulated results, indicating that molecular simulations can guide prescription screening to some extent. In conclusion, our study sheds new light on transdermal immunization via a microneedle therapy.

## ACKNOWLEDGMENTS

The authors gratefully acknowledge financial support from the Young Top Talents of Liaoning Xingliao Talents Program and the Young and Middle-aged Scientific and Technological Innovation Talents Plan in Shenyang.

## FUNDING STATEMENT

This work was supported by the Young Top Talents of the Liaoning Xingliao Talents Program (XLYC2007184) and the Young- and Middle-Aged Scientific and Technological Innovation Talents Plan in Shenyang (RC200367).

## CONFLICT OF INTEREST

The authors declare no competing interests.

## REFERENCES

- Ahmed Saeed Al-Japairai K, Mahmood S, Hamed Almurisi S, Reddy Venugopal J, Rebhi Hilles A, Azmana M, et al. Current trends in polymer microneedle for transdermal drug delivery. *Int J Pharm X*. 2020;587:119673.
- Anderson A, Hegarty C, Casimero C, Davis J. Electrochemically controlled dissolution of nanocarbon-cellulose acetate phthalate microneedle arrays. *ACS Appl Mater Interfaces*. 2019;11(39):35540-35547.
- Balmert SC, Carey CD, Falo GD, Sethi SK, Erdos G, Korkmaz E, et al. Dissolving undercut microneedle arrays for multicomponent cutaneous vaccination. *J Control Release*. 2020;317:336-346.
- Chiu TM, Hsu PC, Khan MY, Lin CJ, Lee CH, Hsu TC, et al. A Perspective on Imiquimod Microneedles for Treating Warts. *Pharmaceutics*. 2021;13(5):607.
- Chiu YH, Chen MC, Wan SW. Sodium Hyaluronate/Chitosan Composite Microneedles as a Single-Dose Intradermal Immunization System. *Biomacromolecules*. 2018;19(6):2278-2285.
- Dharadhar S, Majumdar A, Dhoble S, Patravale V. Microneedles for transdermal drug delivery: a systematic review. *Drug Dev Ind Pharm*. 2019;45(2):188-201.
- Du H, Liu P, Zhu J, Lan J, Li Y, Zhang L, et al. Hyaluronic Acid-Based Dissolving Microneedle Patch Loaded with Methotrexate for Improved Treatment of Psoriasis. *ACS Appl Mater Interfaces*. 2019;11(46):43588-43598.
- Essendoubi M, Gobinet C, Reynaud R, Angiboust JF, Manfait M, Piot O. Human skin penetration of hyaluronic acid of different molecular weights as probed by Raman spectroscopy. *Skin Res Technol*. 2016;22(1):55-62.
- Feng YH, Zhang XP, Li WX, Guo XD. Stability and Diffusion Properties of Insulin in Dissolvable Microneedles: A Multiscale Simulation Study. *Langmuir*. 2021;37(30):9244-9252.
- Hao Feng Y, Ling Liu J, Zhu DD, Hao YY, Dong Guo X. Multiscale simulations of drug distributions in polymer dissolvable microneedles. *Colloids Surf B Biointerfaces*. 2020;189:110844.
- Hoarau A, Polette M, Coraux C. Lung Hyaluronasome: Involvement of Low Molecular Weight Ha (Lmw-Ha) in Innate Immunity. *Biomolecules*. 2022;12(5):658.
- Kim H, Seong KY, Lee JH, Park W, Yang SY, Hahn SK. Biodegradable Microneedle Patch Delivering Antigenic Peptide-Hyaluronate Conjugate for Cancer Immunotherapy. *ACS Biomater Sci Eng*. 2019;5(10):5150-5158.
- Kim NW, Kim SY, Lee JE, Yin Y, Lee JH, Lim SY, et al. Enhanced Cancer Vaccination by In Situ Nanomicelle-Generating Dissolving Microneedles. *ACS Nano*. 2018;12(10):9702-9713.
- La Gatta A, Salzillo R, Catalano C, Pirozzi AVA, D'Agostino A, Bedini E, et al. Hyaluronan-based hydrogels via ether-crosslinking: Is HA molecular weight an effective means to tune gel performance? *Int J Biol Macromol*. 2020;144:94-101.
- Leone M, Priester MI, Romeijn S, Nejadnik MR, Monkare J, O'Mahony C, et al. Hyaluronan-based dissolving microneedles with high antigen content for intradermal vaccination: Formulation, physicochemical characterization and immunogenicity assessment. *Eur J Pharm Biopharm*. 2019;134:49-59.
- Leone M, Romeijn S, Slutter B, O'Mahony C, Kersten G, Bouwstra JA. Hyaluronan molecular weight: Effects on dissolution time of dissolving microneedles in the skin and on immunogenicity of antigen. *Eur J Pharm Sci*. 2020;146:105269.
- Li J, Zeng M, Shan H, Tong C. Microneedle Patches as Drug and Vaccine Delivery Platform. *Curr Med Chem*. 2017;24(22):2413-2422.

- Li Y, Yang J, Zheng Y, Ye R, Liu B, Huang Y, et al. Iontophoresis-driven porous microneedle array patch for active transdermal drug delivery. *Acta Biomater.* 2021;121:349-358.
- Monkare J, Reza Nejadnik M, Baccouche K, Romeijn S, Jiskoot W, Bouwstra JA. IgG-loaded hyaluronan-based dissolving microneedles for intradermal protein delivery. *J Control Release.* 2015;218:53-62.
- Moradi H, Azizpour H, Bahmanyar H, Mohammadi M, Akbari M. Prediction of methane diffusion coefficient in water using molecular dynamics simulation. *Heliyon.* 2020;6(11):e05385.
- Saha I, Rai VK. Hyaluronic acid based microneedle array: Recent applications in drug delivery and cosmetology. *Carbohydr Polym.* 2021;267:118168.
- van der Maaden K, Heuts J, Camps M, Pontier M, Terwisscha van Scheltinga A, Jiskoot W, et al. Hollow microneedle-mediated micro-injections of a liposomal HPV E743-63 synthetic long peptide vaccine for efficient induction of cytotoxic and T-helper responses. *J Control Release.* 2018;269:347-354.
- Vora LK, Courtenay AJ, Tekko IA, Larraneta E, Donnelly RF. Pullulan-based dissolving microneedle arrays for enhanced transdermal delivery of small and large biomolecules. *Int J Biol Macromol.* 2020;146:290-298.
- Wamhoff EC, Schulze J, Bellmann L, Rentzsch M, Bachem G, Fuchsberger FF, et al. A Specific, Glycomimetic Langerin Ligand for Human Langerhans Cell Targeting. *ACS Cent Sci.* 2019;5(5):808-820.
- Wang Z, Wang Y, Bradbury N, Gonzales Bravo C, Schnabl B, Di Nardo A. Skin wound closure delay in metabolic syndrome correlates with SCF deficiency in keratinocytes. *Sci Rep.* 2020;10(1):21732.
- Zhan H, Ma F, Huang Y, Zhang J, Jiang X, Qian Y. Application of composite dissolving microneedles with high drug loading ratio for rapid local anesthesia. *Eur J Pharm Sci.* 2018;121:330-337.
- Zhao Y, Liu D, Tang H, Lu J, Cui F. A MD simulation and analysis for aggregation behaviors of nanoscale zero-valent iron particles in water via MS. *Sci World J.* 2014;2014:768780.
- Zhu J, Tang X, Jia Y, Ho CT, Huang Q. Applications and delivery mechanisms of hyaluronic acid used for topical/transdermal delivery - A review. *Int J Pharm.* 2020;578:119127.
- Zhuang J, Rao F, Wu D, Huang Y, Xu H, Gao W, et al. Study on the fabrication and characterization of tip-loaded dissolving microneedles for transdermal drug delivery. *Eur J Pharm Biopharm.* 2020;157:66-73.
- Zvezdin V, Peno-Mazzarino L, Radionov N, Kasatkina T, Kasatkin I. Microneedle patch based on dissolving, detachable microneedle technology for improved skin quality - Part 1: ex vivo safety evaluation. *Int J Cosmet Sci.* 2020;42(4):369-376.

Received for publication on 20<sup>th</sup> September 2022

Accepted for publication on 20<sup>th</sup> March 2023